Potent antitumor activity of the anti-CD19 auristatin antibody drug conjugate hBU12-vcMMAE against rituximab-sensitive and -resistant lymphomas

Hans-Peter Gerber,[1] May Kung-Sutherland,[1] Ivan Stone,[1] Carol Morris-Tilden,[1] Jamie Miyamoto,[1] Renee McCormick,[1] Stephen C. Alley,[2] Nicole Okeley,[2] Brad Hayes,[3] Francisco J. Hernandez-Ilizaliturri,[4] Charlotte F. McDonagh,[5] Paul J. Carter,[5] Dennis Benjamin,[2] and Iqbal S. Grewal[1]

Departments of [1]Preclinical Therapeutics, [2]Chemistry, and [3]Analytical Biochemistry and Formulations, Seattle Genetics, Bothell, WA; [4]Departments of Medicine and Immunology, Roswell Park Cancer Institute, Buffalo, NY; and [5]Department of Antibody Engineering, Seattle Genetics, Bothell, WA

Despite major advances in the treatment of non-Hodgkin lymphoma (NHL), including the use of chemotherapeutic agents and the anti-CD20 antibody rituximab, the majority of patients eventually relapse, and salvage treatments with non–cross-resistant compounds are needed to further improve patient survival. Here, we evaluated the antitumor effects of the microtubule destabilizing agent monomethyl auristatin E (MMAE) conjugated to the humanized anti-CD19 antibody hBU12 via a protease-sensitive valine-citrulline (vc) dipeptide linker. hBU12-vcMMAE induced potent tumor cell killing against rituximab-sensitive and -resistant NHL cell lines. CD19 can form heterodimers with CD21, and high levels of CD21 were reported to interfere negatively with the activity of CD19-targeted therapeutics. However, we observed comparable internalization, intracellular trafficking, and drug release in CD21^{low} and CD21^{high}, rituximab-sensitive and -refractory lymphomas treated with hBU12-vcMMAE. Furthermore, high rates of durable regressions in mice implanted with these tumors were observed, suggesting that both rituximab resistance and CD21 expression levels do not impact on the activity of hBU12-vcMMAE. Combined, our data suggest that hBU12-vcMMAE may represent a promising addition to the treatment options for rituximab refractory NHL and other hematologic malignancies, including acute lymphoblastic leukemia. (Blood. 2009;113:4352-4361)

Introduction

CD19 is a cell surface receptor expressed from the earliest stages of pre-B-cell development until terminal B-cell differentiation into plasma cells. CD19 acts as a coreceptor, enhancing signaling and antigen processing by the B-cell receptor complex in response to antigen stimulation.[1] CD19 can form heteromeric complexes with 2 other transmembrane proteins, CD81 (TAPA-1) and CD21.[2] Both CD19 and CD81 are critical regulators of B lymphocyte development and maturation.[1,3,4] In contrast, CD21 is not essential for B-cell maturation,[5] and its expression is mostly limited to transitional B cells.[6]

Approximately 15 types of B-cell lymphomas are distinguished in the current World Health Organization lymphoma classification. Among the B-cell lymphoma surface antigens targeted by therapeutic antibodies such as CD20, CD21, CD22, and CD79B, CD19 is the most widely and homogeneously expressed.[7] CD19 is also broadly expressed on chronic lymphocytic leukemia (CLL), pre–B-cell acute lymphoblastic leukemia (ALL)[8,9] and Waldenstrom macroglobulinemia.[10] CD19 is a rapidly internalizing cell surface protein, which is critical for optimal therapeutic effects of antibody drug conjugates. Potent antilymphoma activities associated with complex internalization and intracellular release of free drug were reported for various anti-CD19 antibodies or antibody drug conjugates (ADCs).[11-13] However, the antitumor effects of these anti–CD19-ADCs were variable, suggesting that antibody specific properties, such as epitope binding, the ability to induce CD19 oligomerization and differences in intracellular signaling, may affect ADC potencies.[9,13-17]

The anti-CD20 antibody rituximab (Rituxan) is used for the treatment of nearly all types of B-cell non-Hodgkin lymphoma (NHL) as first-line therapy in combination with "standard of care" chemotherapy, or as single agent and is also increasingly used as maintenance therapy.[18] Despite encouraging clinical results, retreatment of patients with indolent lymphomas with single-agent rituximab was associated with a response rate of only 40%, suggesting that resistance may occur as a response by malignant B cells to prolonged exposure to rituximab.[19-21] Importantly, rituximab-resistant cell lines generated in vitro display cross-resistance when tested against a panel of chemotherapeutic agents because of a block in the cell apoptosis pathway.[22-24] Several groups recently reported that such cross-resistance in NHL cell lines is associated with alterations in the expression levels of the antiapoptotic proteins Bcl-2, and Bcl-xL[25,26] and the proapoptotic proteins Bax and Bak.[24] Combined, these observations provide a strong rationale for the development of novel therapeutics that are not affected by these molecular changes to successfully treat de novo and rituximab-resistant NHL.

A recent study suggested that high levels of endogenously or exogenously expressed CD21 may limit the internalization and cell killing of anti-CD19 ADCs against human lymphoma cell lines grown in culture.[15] However, flow cytometry and coimmunoprecipitation experiments with patient tumor cells or cultured lymphoma

Submitted September 17, 2008; accepted December 31, 2008. Prepublished online as *Blood* First Edition paper, January 15, 2009; DOI 10.1182/blood-2008-09-179143.

The online version of this article contains a data supplement.

The publication costs of this article were defrayed in part by page charge payment. Therefore, and solely to indicate this fact, this article is hereby marked "advertisement" in accordance with 18 USC section 1734.

cell lines revealed that CD19 is expressed at higher levels compared with CD21, indicating that the majority of CD19 is present in the uncomplexed form.[27,28] Therefore, it remained unclear to what extent high CD21 expression levels may affect the potencies of an anti-CD19–auristatin conjugate.

In this report, we describe a novel, humanized anti-CD19 antibody drug conjugate (hBU12-vcMMAE), consisting of the tubulin-destabilizing auristatin derivative MMAE. The linker type used for conjugation is the dipeptide linker valine-citrulline (vc), which is a proteolytic substrate for cathepsin B, an enzyme that is present in the lysosomal compartment of cells.[29] We demonstrate that hBU12-vcMMAE internalizes to the lysosomal compartment, leading to the release of free, active drug and inhibition of rituximab-sensitive and -resistant, as well as $CD21^{low}$ and $CD21^{high}$ tumors.

Methods

Cell lines and reagents

Cell lines were obtained from ATCC (Manassas, VA) or Deutsche Sammlung von Mikroorganismen und Zellkulturen (Braunschweig, Germany) and cultured in a tissue culture incubator at 37°C according to the recommendations of the cell provider. The murine BU12 was selected from a panel of several anti-CD19 antibodies previously described in the literature based on our observation of its superior internalization kinetics and therapeutic activity when conjugated to auristatin drugs and tested on a panel of human NHL cell lines in vitro (D.B., unpublished data, 2006). The human CD19-selective BU12 was originally generated by immunization of mice with the Burkitt lymphoma cell line EB4.[30] The humanized anti-CD19 antibody, hBU12, showed comparable antigen-binding activity to BU12 in competition-binding assays conducted with $CD19^+$ Ramos cells. The hBU12-vcMMAE(4) conjugate was synthesized by conjugation of an average of 4 MMAE molecules to the cysteine residues that compose the interchain disulfides of hBU12 via a protease cleavable vc linker as described previously.[31,32] The Raji cell lines Raji-2R and Raji-4RH were generated from the parental clone as described previously,[22] with Raji-2R and -4RH being selected for rituximab resistance in the presence or absence of complement in the culture medium, respectively. Both rituximab-resistant clones displayed significantly reduced levels of the proapoptotic proteins Bax, Bak, and Bcl-XL when analyzed by Western blotting[24] (Figure 5C).

Flow cytometric analysis to determine CD19 and CD21 copy numbers

Cells were incubated for 30 minutes on ice with *Pseudomonas exotoxin* (PE)–conjugated murine anti-CD19 and anti-CD21 antibodies (BD Biosciences PharMingen, San Diego, CA), washed with cold staining medium, and evaluated with a BD Biosciences FACScan flow cytometer (San Jose, CA). Quantification of CD19 and CD21 copy numbers on the cell surfaces was determined using a Dako QiFiKit flow cytometric indirect immunofluorescence assay as described by the manufacturer (Dako, Glostrup, Denmark).

Saturation binding studies to determine binding affinity

Cells were incubated with 10 μg/mL AlexaFluor-488–labeled hBU12 antibody or hBU12-vcMMAE for 1 hour at 4°C, and rinsed with cold phosphate-buffered saline (PBS). Binding was assessed using a BD Biosciences FACScan flow cytometer. The apparent Kd values were determined using the One Site Binding algorithm from Prism (GraphPad Software, San Diego, CA).

CD19 internalization kinetic studies

Cells were incubated with 10 μg/mL hBU12 or hBU12-vcMMAE for 30 minutes on ice, rinsed with ice-cold PBS, and resuspended in growth medium. One set of cells was kept at 4°C, and another set was transferred to 37°C. Samples were harvested at the indicated time points and processed for flow cytometry. To detect surface-bound antibody or ADCs, cells were incubated with goat antihuman IgG-fluorescein isothiocyanate-conjugated antibody (Jackson ImmunoResearch Laboratories, West Grove, PA), and binding was assessed using a BD Biosciences FACScan.

ADC drug release studies

Custom-synthesized [^{3}H]-mc-vcMMAE (24.7 Ci/mmol; Moravek Biochemicals, Brea, CA) was used to prepare radiolabeled hBU12-vcMMAE conjugates. Conjugation was carried out using a method similar to that described previously[31] using a mixture of unlabeled mc-vcMMAE and ^{3}H-mc-vcMMAE in a proportion determined to generate drug conjugates with a specific activity of approximately 30 μCi/mg. The drug loading was estimated using reverse phase (PLRP) chromatography,[31] and the specific activity of the conjugate was determined by ultraviolet/visible spectroscopy and liquid scintillation counting (LSC). To determine the free drug release, cells were seeded at 5×10^5 cells/mL. Radioactive ADC was added to each culture at a final concentration of 200 ng/mL. After mixing, aliquots were removed as a reference for the total amount of radioactivity added to the culture. On each day of the 3-day experiment, cell densities and viabilities were determined by trypan blue exclusion. At certain time points, the cultures were mixed and aliquots were removed and centrifuged at 390*g* for 3.5 minutes at room temperature. An aliquot of the supernatant was removed for further analysis, and the pellet was washed twice with ice-cold PBS. The cells were resuspended in 100 μL of complete medium and treated with 900 μL of ice-cold methanol to precipitate protein and to permeabilize the cells. The samples were stored at −20°C for more than or equal to 30 minutes before centrifugation at 16 000*g* for 5 minutes. The entire supernatant was examined by LSC. A sample of the culture medium from each time point was diluted 9-fold with ice-cold methanol. The suspension was stored at −20°C for more than or equal to 30 minutes and subsequently centrifuged at 16 000*g* for 5 minutes. A sample of the supernatant was counted by LSC. All samples used for LSC were mixed with 4 mL of scintillation fluid (Ecoscint A; National Diagnostics, Atlanta, GA).

The radioactivity calculations were made after subtracting background from all disintegrations per minute (dpm) values. The background-corrected dpm values were first converted to μCi and then to pmol of drug, using the specific activity of the radioactive ADC and its drug loading. The concentration of total drug released in the cell culture was determined from the amount of free drug found inside of the cells grown in 1 mL of culture medium combined with the amount detected in 1 mL of culture medium. Triplicate results were averaged, and the SD for those values was calculated using the STDEVPA function in Microsoft Excel (Redmond, WA).

Lysosomal colocalization studies of hBU12 and hBU12-ADCs

Cells were kept on ice in the presence of 1 μg/mL hBU12 or hBU12-vcMMAE and then incubated for 20 minutes or 4 hours at 37°C. After the incubation, the cells were washed with cold PBS to remove unbound antibody or ADC and then fixed and permeabilized with BD Cytofix/Cytoperm (BD Biosciences). The antibody and ADCs were detected with AlexaFluor-488–labeled goat anti–human IgG (Invitrogen, Carlsbad, CA). Lysosomal compartments were visualized by staining with AlexaFluor-647–labeled LAMP-1 antibody (mouse CD107, BD Biosciences). Nuclear compartments were stained with 4′,6-diamidino-2-phenylindole (Roche Diagnostics, Basel, Switzerland). Fluorescence images were acquired with a Zeiss Axiovert 200M microscope (Carl Zeiss, Thornwood, NY) at a 63× magnification. Specimens were mounted in Vectashield Mounting Medium (Vector Laboratories, Burlingame, CA). Pictures were taken with a Zeiss AxioCam CCD camera, using Axiovision imaging software (Carl Zeiss).

Cytotoxicity assays

Tumor cells were incubated with hBU12 or drug conjugates for 96 hours. Cell viability was measured by Alamar Blue (BioSource International, Camarillo, CA) dye reduction as reported previously.[33] Cells were incubated for 4 hours with the dye, and dye reduction was measured on a Fusion HT fluorescent plate reader (PerkinElmer Life and Analytical Sciences, Waltham, MA). Results are reported as IC_{50}, the concentration of compound needed to yield a 50% reduction in viability compared with vehicle-treated cells (control = 100%).

Western blotting analysis of Bcl-2 family members

Cell lysates were prepared from Ramos, Raji, and their rituximab-resistant cell lines cultured in RPMI growth media containing 2% heat-inactivated FBS and treated for 48 hours with vehicle or rituximab (10 μg/mL). Rituximab was cross-linked by incubating the antibody with goat antihuman IgG (Jackson ImmunoResearch Laboratories) at a 1:4 ratio for 20 minutes at room temperature before addition to cells. Cell lysates were run on 4% to 20% gradient Tris-Gly mini-gels (Invitrogen), transferred onto polyvinyl difluoride (PVDF) membranes (Invitrogen), and blotted with antibodies to Bak (Upstate Biotechnology, Charlottesville, VA), Bax (BD Biosciences), Bcl-2, and Bcl-XL (Cell Signaling Technology, Danvers, MA). Detection was performed using horseradish peroxidase-conjugated goat anti–mouse or goat anti–rabbit secondary antibodies (Jackson ImmunoResearch Laboratories) and chemiluminescent reagents (Supersignal West Pico; ThermoScientific, Rockford, IL).

In vivo model of subcutaneous lymphomas and disseminated human leukemias

All animal experiments were conducted in an Association for Assessment and Accreditation of Laboratory Animal Care–accredited facility and under Institutional Animal Care and Use Committee guidelines and approval. Localized and disseminated models of B-cell lymphomas were established in female C.B-17 severe combined immunodeficiency (SCID) mice (Harlan, Indianapolis, IN). For the subcutaneous model, 5×10^6 cells were implanted into the right flank of female mice. hBU12-vcMMAE or a control, nonbinding ADC as indicated, were administered when average tumor volumes reached 100 mm^3; tumor size was monitored at least twice weekly. For the disseminated model of disease, 5×10^6 tumor cells were inoculated intravenously into the lateral tail vein of SCID mice. Animals were observed and killed when evidence of disease, such as hind limb paralysis or a weight loss of 15% to 20%, was evident. More than 90% of the untreated, lymphoma-bearing mice required death within 40 to 60 days after tumor cell implantation as the result of disease development. Mice were treated with test compounds 7 days after injection of the tumor cells. Treatment schedules were as indicated in the figure legends.

Development of rituximab-resistant Ramos tumors

Parental, rituximab-sensitive tumor cells were implanted into SCID mice at a concentration of 5×10^6 cells per mouse. Two days after cell implant, mice were treated with rituximab at 8 mg/kg every other day for a total of 9 doses. Of the 40 implanted animals, 6 developed tumors. When the tumors reached approximately 300 to 400 mm^3, mice were killed and tumors were collected aseptically. Tumors were made into a single-cell suspension through dissociation using a nylon filter. While in culture, the cells were continuously exposed to increasing amounts of rituximab, reaching up to 100 μg/mL. Cell viability was verified several times per week for several weeks, and thereafter cells were implanted into secondary recipient SCID mice. Two days after cell implant, tumors were treated with rituximab at 12 mg/kg, 3 times weekly. The selection procedure described was repeated twice to result in R-Ramos. The resulting tumors were processed into single-cell suspension and frozen in liquid nitrogen. In all xenograft experiments shown, the drug was administered intraperitoneally.

Statistical analysis

Tumor quadrupling times were chosen as time to endpoint (TTE) and were determined using a nonlinear regression analysis for exponential growth of each individual tumor growth dataset from each experimental animal. The tumor quadrupling time was calculated for each tumor based on the tumor volume at the beginning of treatment. Percentage tumor growth delay (% TGD) represents the delay in reaching TTE relative to control tumors, which was determined using the formula: $\%\ TGD = [(T - C)/C] \times 100$, where T and C are the median times in days for treated and control groups, respectively, to reach TTE, using the start of treatment as day 1.[34] Animals that did not reach tumor quadrupling were assigned a TTE value equal to the last day of the study. Statistical analysis and graphic presentations were conducted using GraphPad Prism Software version 4.01 (GraphPad Software, La Jolla, CA). Log-rank test (Mantel-Cox) was used to analyze the significance of the differences between TTE of treated and control tumor groups, with differences deemed significant at P values less than or equal to .05 and highly significant at P values less than or equal to .005.[34] In a complete response (CR), the tumor volume remained undetectable (0 mm^3) for 3 consecutive measurements during the course of the study. A durable response (DR) is defined as complete absence of palpable tumor during the entire experiment as described previously.[34] The experimental cohorts in subcutaneous tumor implant models contained 8 to 10 mice, and 10 mice for the disseminated tumor models. Tumor growth curves show shown represent mean tumor volumes as a function of time plus or minus SEM. To determine the significance of correlations between CD19 and CD21 expression levels and in vitro cytotoxicity, standard Pearson correlation analysis (2-tailed) was used with a 95% confidence interval.

Results

Among the most critical properties that determine the ability of ADCs to interfere with tumor growth is the binding affinity to their respective tumor antigen, rapid internalization kinetics, and subcellular trafficking to the lysosomal compartment.[35] To investigate the effects of the humanization and conjugation processes of hBU12 on binding to its target antigen, cell-binding experiments were conducted with $CD19^+$ 293F cells, stably expressing human CD19. BU12, hBU12, and the hBU12-vcMMAE conjugate all bound hCD19 with comparable affinities, at apparent Kd values of 1.7, 2.2, and 3.4 nM, respectively. Next, we exposed $CD19^+$ human lymphoma and leukemia cell lines to increasing concentrations of hBU12-vcMMAE or the free drug (MMAE) to determine the IC_{50} values for tumor growth inhibition (Table 1). The cell lines tested represent Burkitt lymphoma (CA46, Namalwa, Ramos, Daudi, Raji), diffuse large B-cell lymphomas (DLBCLs; HT, RL, WSU-DLCL2, SUDHL-6, SUDHL-4), transformed follicular lymphomas (DOHH2, WSU-NHL), a large B-cell lymphoma (ARH-77), CLL (MEC-2, JVM3), and ALL (Nalm-6, RS4;11). In addition, we determined the cell surface copy numbers of CD19 and CD21 by quantitative FACS analysis to study a potential correlation between expression of both genes and activity of hBU12-vcMMAE (Table 1). Potent cytotoxic effects by hBU12-vcMMAE were noticed in 15 of 17 $CD19^+$ tumor cell lines tested. The lower potency of hBU12-vcMMAE against the RL and MEC-2 tumor cell lines does not reflect a general resistance toward antineoplastic agents of these cell lines, as they were efficiently killed by the anti-CD20 antibody, rituximab (data not shown).[36,37] As shown in Table 1, a lack of correlations between the sensitivity of tumor cells toward hBU12-vcMMAE and free MMAE was noticed, suggesting that potential intrinsic differences in the sensitivity of tumor cells toward MMAE may not account for the potency differences. As a negative control cell line, we used the CD19-deficient T-cell lymphoma cell line Jurkat. The absence of activity against these control cells suggested that the antitumor effects of hBU12-vcMMAE are immunologically specific. Both unconjugated hBU12 and a control, nonbinding vcMMAE conjugate exhibited negligible antitumor activities when tested against these cell lines (data not shown). Despite such target antigen requirement for hBU12-vcMMAE to kill tumor cells, a lack of significant correlations between CD19 expression levels and ADC potency was noticed ($P = .45$, $R^2 = 0.038$, standard Pearson analysis). Similarly, a lack of correlation between CD21 levels and potency was also found ($P = .55$, $R^2 = 0.028$). Combined, these findings suggest that neither CD19 nor CD21 expression levels predict the sensitivities of lymphoma and leukemia cell lines toward hBU12-vcMMAE. In addition, we found comparable IC_{50} values of hBU12-vcMMAE for NHL and ALL cell

Table 1. CD19 and CD21 expression levels and cytotoxicity of hBU12 -vcMMAE against ALL, CLL, and NHL tumor cell lines grown in culture

Tumor type / cell line	CD21, copy no.	CD19, copy no.	IC_{50}, nM hBU12-vcMMAE	IC_{50}, nM free MMAE
ALL				
Nalm-6	0	53773	4.0 ± 0.05	0.65 ± 0.07
RS4;11	0	38227	0.050 ± 0.007	0.080 ± 0.007
Transformed follicular lymphoma				
DOHH2	0	40056	4.5 ± 0.7	0.200 ± 0.005
WSU-NHL	0	36242	0.35 ± 0.07	0.200 ± 0.005
DLBCL				
HT	952	36834	0.20 ± 0.04	0.103 ± 0.002
RL	0	32542	> 300	0.25 ± 0.07
WSU-DLCL2	0	19924	51 ± 0.71	0.30 ± 0.01
SUDHL-6	0	13784	0.04 ± 0.01	0.136 ± 0.003
SUDHL-4	0	38932	99 ± 15	0.71 ± 0.07
Burkitt				
CA46	2167	57240	1.4 ± 0.8	0.53 ± 0.09
Namalwa	374	28629	45 ± 29	0.31 ± 0.10
Ramos	2369	41016	0.60 ± 0.28	0.15 ± 0.01
Daudi	25531	54074	30 ± 2	0.193 ± 0.007
Raji	56660	78798	33.3 ± 7.1	0.43 ± 0.06
Large B-cell lymphoma				
ARH-77	29537	54324	126 ± 31	0.63 ± 0.16
CLL				
MEC-2	33246	67562	> 300	2 ± 0.6
JVM3	17850	26321	42 ± 5	0.20 ± 0.07
T-cell leukemia				
Jurkat: $CD19^-$	> 300	0	> 300	0.25 ± 0.04

IC_{50} values were determined by incubation of the tumor cell lines for 96 hours to the hBU12-vcMMAE conjugate or MMAE, as indicated. Cell lines, in which less than 50% cytotoxicity was achieved at concentrations greater than or equal to 300 nM, were considered nonresponsive. Both unconjugated hBU12 and a control, nonbinding vcMMAE conjugate exhibited negligible antitumor activities against these cell lines. All values obtained for hBU12-vcMMAE are significantly different from control-vcMMAE compounds tested in the same assay (Student *t* test, data not shown). Jurkat cells were used as a $CD19^-$ control cell line. The absence of activity of hBU12-vcMMAE on these control cells suggested that the antitumor activity is immunologically specific. Data shown represent the mean plus or minus SD of three replicates from 2 independent experiments.

lines, demonstrating broad antitumor effects of hBU12-vcMMAE in various B-cell malignancies.

Internalization kinetics and intracellular trafficking of hBU12-vcMMAE in NHL cell lines

A key parameter determining the antitumor activities of auristatin-based ADCs is their ability to internalize and to translocate to the lysosomal compartment after antigen binding.[29,35] To study these processes, we incubated $CD21^{low}$ (Ramos, Nalm-6) and $CD21^{high}$ tumor cell lines (Raji, Daudi) with hBU12 and hBU12-vcMMAE and determined the internalization kinetics by measuring their disappearance from the cell surface by flow cytometry. As shown in Figure 1A, B, the majority of hBU12-vcMMAE conjugates internalized on $CD21^{low}$ Ramos and Nalm6 cells within 2 hours after incubation. Interestingly, hBU12 internalization was less efficient in Nalm-6 cells compared with the hBU12-vcMMAE conjugate. The nature of these differences is unclear; however, similar effects were observed previously with rituximab-vcMMAE[8] conjugates, where the conjugated form of the antibody internalized more efficiently compared with rituximab.[38] Comparable internalization kinetics for hBU12-vcMMAE was noticed between $CD21^{low}$ Ramos and Nalm-6 cells (Figure 1A,B) and $CD21^{high}$ Raji and Daudi cells (Figure 1C,D). We noticed a trend toward increased levels of noninternalizing compounds on $CD21^{high}$ tumor cells. However, these differences did not alter the activity of hBU12-vcMMAE, as similar IC_{50} values were measured in $CD21^{low}$ Nalm-6 and Ramos cells compared with $CD21^{high}$ lymphoma cells (Table 1). Therefore, our findings suggest that potential differences in the internalization kinetics of hBU12-vcMMAE may not account for the potency variations found between different NHL cell lines.

To investigate the intracellular trafficking of hBU12 and hBU12-vcMMAE conjugates, we incubated $CD21^{low}$ Ramos cells with either hBU12 or hBU12-vcMMAE. Coimmunofluorescence studies revealed that the majority of internalized hBU12 localized to lysosomes, starting as early as 15 minutes after incubation (data not shown) and with high levels of colocalization reached after 24 hours of incubation (Figure 2A). Comparable levels of hBU12 and hBU12-vcMMAE localized to the lysosomal compartment in $CD21^{low}$ Ramos and $CD21^{high}$ Daudi and Raji cells. A lack of staining with a nonbinding control mAb and absence of lysosomal localization was noticed with a mAb targeting a noninternalizing antigen (Figure S1, available on the *Blood* website; see the Supplemental Materials link at the top of the online article). Combined, these findings demonstrate the requirements for selective antigen binding for internalization and lysosomal trafficking and immunologic specificity of ADCs. In conclusion, our findings demonstrate that differences in internalization kinetics can be ruled out to cause the differences in potency of hBU12-vcMMAE against different NHL cell lines.

Free drug release by hBU12-vcMMAE in rituximab-sensitive and -resistant $CD21^{high}$ and $CD21^{low}$ lymphoma cell lines

MMAE interferes with microtubule stability within the cytoplasmic compartment of cells; thus, the amounts of free, active MMAE drug released within tumor cells may be critical for antilymphoma activity.[33] To investigate these aspects, we tested hBU12-vcMMAE against $CD21^{low}$ Ramos, $CD21^{high}$ Daudi, and $CD21^{high}$, rituximab-resistant Raji-2R and -4RH cell lines and compared the amounts of free drug released over time by measuring the radioactivity within cells and in the supernatant (released from cells). As shown in

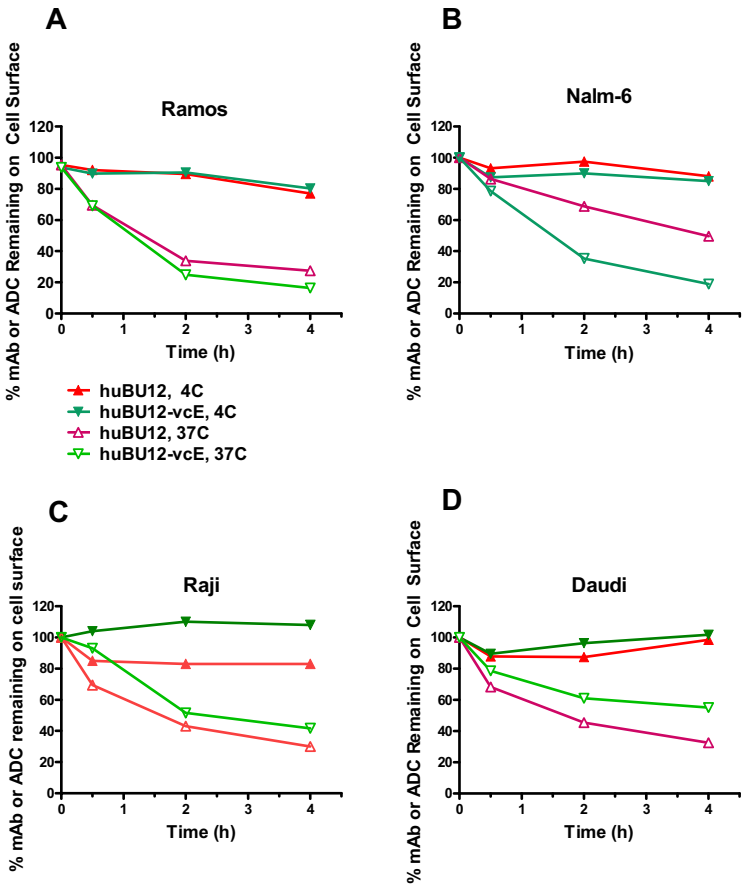

Figure 1. Internalization kinetics of hBU12 and hBU12-vcMMAE on NHL and ALL tumor cell lines. Internalization kinetics of hBU12 and hBU12-vcMMAE was determined by flow cytometry of CD21^{low} (A) Nalm-6 and (B) Ramos cells. The majority of the compounds disappeared from the cell surface within 1 to 2 hours after incubation. Internalization kinetics of hBU12 and hBU12-vcMMAE on CD21^{high} (C) Raji and (D) Daudi cells. Similar to our findings with CD21^{low} cells, the majority of the compounds internalized within 1 to 2 hours of incubation of CD21^{high} cell lines. However, the fraction representing the noninternalized compounds was higher in CD21^{high} compared with CD21^{low} cells after 4 hours of incubation.

Figure 2B, C and Table 2, comparable amounts of free MMAE accumulated over a 72-hour time period by rituximab-sensitive and -resistant, CD21^{high} and CD21^{low} tumor cells. Therefore, potential variations in free drug release are unlikely to account for the more than 50-fold differences in the IC_{50} values between lymphoma cell lines (Table 1). In conclusion, high CD21 expression levels or rituximab resistance may have minimal effects on the release of free drug from hBU12-vcMMAE conjugates and cytotoxicity.

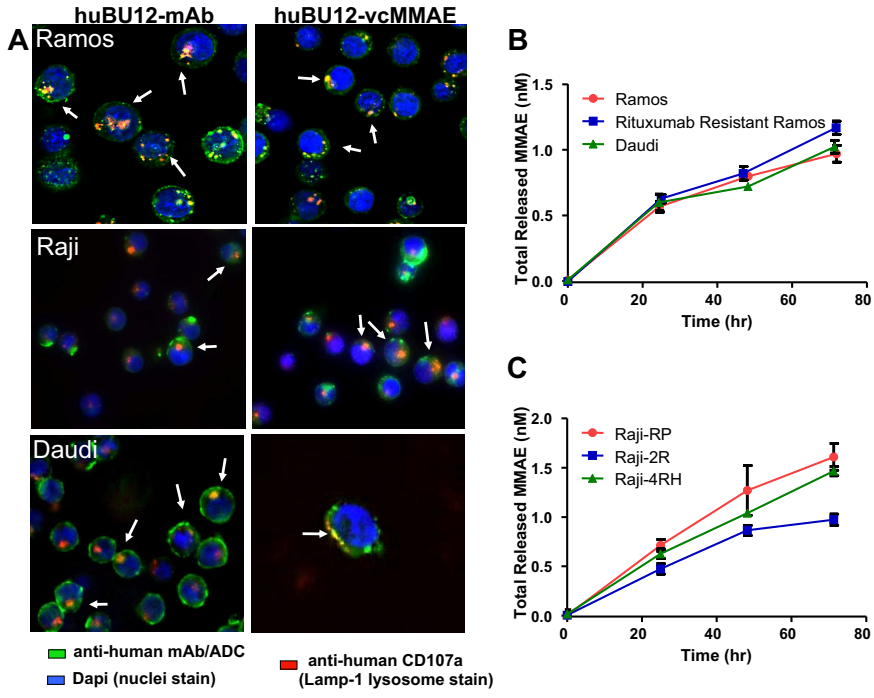

Figure 2. Immunohistochemical analysis of the subcellular localization of hBU12 and hBU12-vcMMAE in lymphoma cell lines. Twenty-four hours after incubation at 37°C, cells were fixed, permeabilized, and stained with the LAMP-1 lysosomal antibody (red) and/or antibodies binding to hBU12 (left panels) and hBU12-vcMMAE (right panels, green). Control reagents included a vcMMAE or mAb that did not internalize or a nonbinding molecule, which both failed to localize to the lysosomes (see Figure S1). (A) Immunohistochemical analysis of CD21^{low} Ramos cells and CD21^{high} Raji and Daudi cells. The hBU12 conjugates mostly localized within the lysosomal compartment, as indicated by the yellow staining pattern. Arrows show colocalization of ADCs with lysosomes. We were unable to identify differences in the proportion of compounds localizing to the lysosomal compartment between CD21^{high} and CD21^{low} cells. (B) Amounts of total free drug released over time from CD21^{low} Ramos, CD21^{high} Daudi, and rituximab-resistant Ramos cells. (C) Levels of free drug released over time in CD21^{high}, parental Raji-RP cells, and rituximab-resistant Raji-2R and Raji-4RH cells. Reduced amounts of free MMAE were observed in Raji-2R, but not Raji-4RH cells, relative to the parental Raji-RP cells.

Table 2. Levels of free drug release in CD21^{high} and CD21^{low} lymphoma cell lines

Cell line	Rituximab-resistant	Percentage of total ADC turnover
Ramos (CD21^{low})	No	22
R-Ramos (CD21^{low})	Yes	21
Daudi (CD21^{high})	No	26
Raji (CD21^{high})	No	25
Raji-2R (CD21^{high})	Yes	19
Raji-4RH (CD21^{high})	Yes	26

Rituximab-resistant (Raji-2R, -4RH, R-Ramos) or -sensitive (Ramos, Daudi) cells were treated with hBU12-vcMMAE made with radioactively labeled MMAE (hBU12-vcMMAE*, ~ 4 drugs/mAb). The total amount of released MMAE over time was determined by methanol precipitation and liquid scintillation counting, providing the nmol of drug released per volume of cell culture. Data are expressed as percentage ADC cleaved relative to the total amount of ADC added to the cells. Comparable levels of released free MMAE and total ADC turned over were observed in all cell lines tested. Data shown represent the mean of 2 replicates of one representative of 2 independent experiments.

Efficacy of hBU12-vcMMAE in models of NHL and ALL

Ultimately, we were interested to test the antitumor effects of hBU12-vcMMAE in preclinical models of NHL and ALL. For this purpose, we tested hBU12-vcMMAE in single-dose (data not shown) and multidose experiments against different NHL and ALL xenografs (Figures 3-5). The pharmacokinetic properties of hBU12-vcMMAE were determined using a noncompartmental analysis method of serum samples. The half-life of hBU12-vcMMAE conjugates in SCID mice was calculated to be approximately 7 days, which is comparable with other vcMMAE antibody drug conjugates reported previously (Table S1).[39] When tested against DOHH2 tumors (transformed follicular lymphoma), significant inhibition of tumor growth and 2 of 10 DRs (Figure 3A, $P < .001$ vs hBU12 and untreated) were observed at the 3-mg/kg dose level. Similarly, 2 of 10 DRs were found with DLCL2 tumors (DLBCLs) treated at the 3-mg/kg dose level (Figure 3B, $P < .001$ vs hBU12 and untreated). In the disseminated RS4;11 tumor model (ALL), a significant increase in survival of mice treated with hBU12-vcMMAE was noticed, and a delay in disease onset between control and untreated animals at the 3 mg/kg dose level, from approximately 45 to more than 90 days was found, with 3 of 10 animals remaining disease free at the end of the experiment (Figure 3C, $P < .001$ vs untreated and control ADC). Similar observations were made in a second disseminated model of ALL

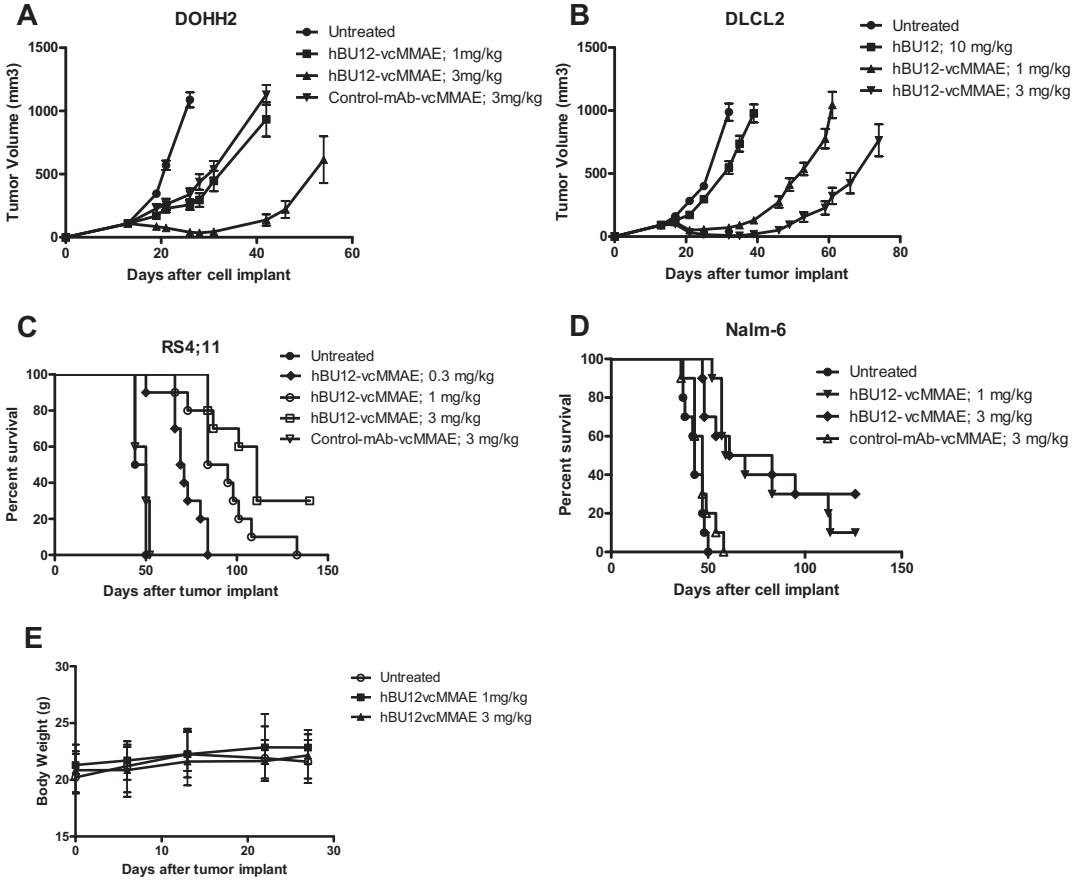

Figure 3. Xenograft experiments testing hBU12-vcMMAE in models of NHL. In the subcutaneous xenograft models, treatment with hBU12-vcMMAE, or hBU12 or control compounds, was initiated when the average tumor volume per experimental cohort reached 100 mm^3. Naked hBU12 failed to induce significant antitumor effects in the models shown (A; and data not shown). Mice were treated with hBU12-vcMMAE or control compounds at 1 and 3 mg/kg, q4dx4, via intraperitoneal administration. In all experiments, hBU12-vcMMAE significantly reduced tumor burden and improved survival compared with untreated mice or mice treated with hBU12 mAb or control-vcMMAE antibody. (A) Tumor growth curve of the follicular lymphoma cell lines DOHH2 treated with hBU12-vcMMAE at the dose and schedule indicated. (B) Tumor growth curve of the DLBCL cell line, DLCL2, treated with hBU12-vcMMAE at the dose and schedule indicated. (C) Survival of mice implanted with RS4;11 cells (ALL) via tail vein injections. Treatment of mice was initiated on day 7 after tumor implantation. (D) Survival curve of mice implanted with Nalm-6 cell (ALL) via tail vein injections. In the disseminated model, treatment was initiated on day 7 after tumor implantation. Data shown in panels A to D are from one representative of at least 2 independent experiments conducted. The graphs showing tumor volumes over time display median ± SEM of experimental cohorts of 7 to 10 animals. (E) Body weight changes of mice implanted intravenously with Nalm-6 tumor cells, with dosing starting on day 7 after tumor implantation (q4dx4), with the last dose administered on day 19. No significant changes in body weights between experimental cohorts by treatment were found in all xenograft experiments (data not shown). Data shown represent mean plus or minus SEM of experimental cohorts of 10 animals.

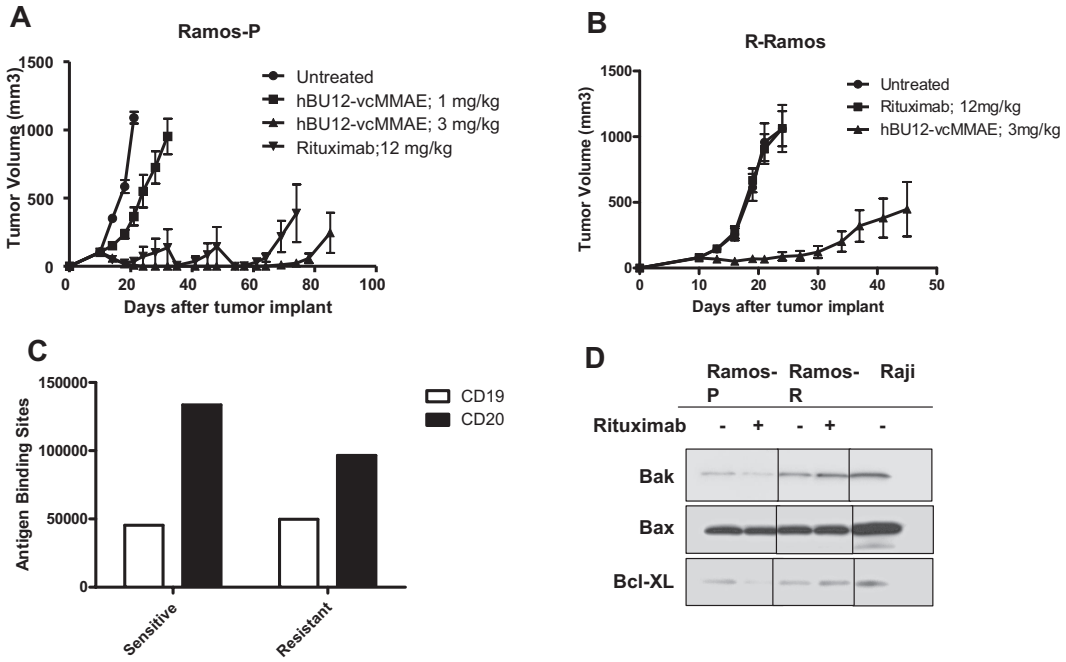

Figure 4. Efficacy of hBU12-vcMMAE in rituximab-resistant lymphomas. (A) Tumor growth curves of parental Ramos cells used to generate rituximab-resistant (R-Ramos) tumors. Tumor growth was significantly reduced by both rituximab (12 mg/kg, q4dx4) and hBU12-vcMMAE (3 mg/kg, q4dx4) treatment. The 2 peaks in the rituximab group were caused by the removal of 2 animals with tumors sizes exceeding 1000 mm^3. (B) Tumor growth curves of rituximab-resistant R-Ramos tumors treated with hBU12-vcMMAE (3 mg/kg, intraperitoneally, q4dx4) or rituximab (12 mg/kg, q4dx4, intraperitoneally). hBU12 mAb failed to induce significant tumor growth delay in Ramos and R-Ramos (data not shown). Data shown in panels A and B are from one representative of 2 independent experiments, with 8 to 10 animals per group. (C) Flow cytometry to determine CD19 and CD20 expression levels on cells isolated from Ramos-P (sensitive) and R-Ramos (resistant) tumors. Comparable expression levels of both antigens were identified. (D) Western blot analysis of Bax, Bcl-XL, and Bak expression in rituximab-resistant Ramos cells (R-Ramos) or rituximab-sensitive, parental tumor cells (Ramos). Vertical lines have been inserted to indicate repositioned gel lanes.

(Nalm-6), where 3 of 10 mice treated at doses of 3 mg/kg remained disease free (Figure 3D, $P < .001$ vs untreated and control ADC). Consistent with the previously published maximal tolerated dose (MTD) for vcMMAE conjugates of more than 50 mg/kg in mice,[40] single-dose administration of 1 and 3 mg/kg, 4 doses every 4 days (q4dx4) of hBU12-vcMMAE was not associated with any significant

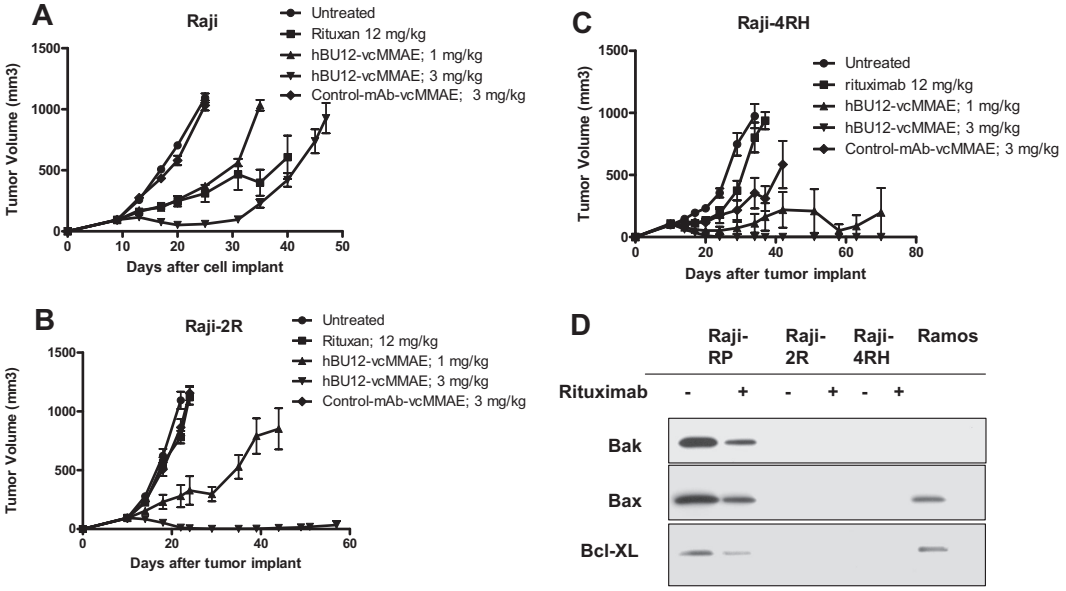

Figure 5. Antilymphoma effects of hBU12-vcMMAE against subcutaneously implanted, rituximab-resistant Raji tumors. (A) Parental Raji tumors were treated with rituximab (12 mg/kg, 3 times weekly), hBU12-vcMMAE (q4dx4), or control-vcMMAE compound. (B) Raji-2R tumors treated with hBU12-vcMMAE at 1 or 3 mg/kg, q4dx4 or a control conjugate. Nine durable regressions in 10 tumor-bearing mice were obtained after hBU12-vcMMAE treatment, whereas rituximab (12 mg/kg, 3 times weekly for 2 weeks) did not significantly impact tumor growth. (C) Effect of hBU12-vcMMAE treatment (q4dx4) on growth of subcutaneously implanted Raji-4RH tumors. For comparison, control groups were either untreated or treated with a control ADC or with rituximab (12 mg/kg, 3 times weekly for 2 weeks). Data shown in panels A to C are from one representative of 2 independent experiments, with 8 to 10 animals per group. (D) Western blotting analysis of Bax, Bak, and Bcl-XL in cell lysates prepared from Raji-2R or Raji-4RH cell treated with control mAb or rituximab and compared with parental, Raji-P cells and Ramos. Our data confirm the down-regulation of Bax, Bak, and Bcl-XL in rituximab-resistant Raji cell lines reported previously.[24]

changes in body weights or overt toxicity in tumor-bearing animals (Figure 3E; data not shown). Combined, these experiments revealed robust antitumor activities by hBU12-vcMMAE against a variety of $CD19^+$ NHL and ALL tumors, at well tolerated dose levels.

Durable responses by hBU12-vcMMAE against rituximab-resistant lymphoma cell lines

To develop a preclinical model that mimics the rituximab resistance frequently associated with lymphoma patients, Ramos tumor cells were repeatedly passaged in mice and concomitantly treated with rituximab to generate R-Ramos. In subcutaneously implanted tumors, rituximab treatment resulted in a significant increase in tumor growth delay between parental Ramos tumors (Figure 4A; 4 of 8 CRs, 3 DRs, $P < .001$ vs control), but not when tested against rituximab-resistant R-Ramos (Figure 4B; 0 of 8 CRs, $P = .97$ vs control). In contrast, there was significant antitumor activity of hBU12-vcMMAE (3 mg/kg, q4dx4) against rituximab-sensitive (Figure 4A; 6 of 8 CRs, 2 DRs, $P < .001$ vs control) and -resistant Ramos tumors (Figure 4B, 4 of 8 CRs, 2 DRs, $P < .001$ vs control), indicating that the mechanisms associated with rituximab resistance do not markedly affect the activity of hBU12-vcMMAE. To monitor CD19 and CD20 expression levels, we isolated cells from rituximab-resistant (R-Ramos) and parental tumors. Comparable expression levels for CD20 and CD19 were found in rituximab-resistant and -sensitive Ramos tumors when analyzed by flow cytometry (Figure 4C). Western blot analysis of parental and R-Ramos cells revealed alterations in the expression of the Bcl-2 family members Bak and BcL-XL, but not Bax (Figure 4D). Similar alterations were reported previously for rituximab-resistant Ramos cells.[23] Furthermore, potent antilymphoma activities of hBU12-vcMMAE against rituximab-sensitive Raji tumors (Figure 5A; 1 of 10 DRs, $P < .001$ vs control) and -resistant Raji-2R (Figure 5B; 9 of 10 DRs, $P < .001$ vs control) and Raji-4RH tumors (Figure 5C; 9 of 10 DRs, $P < .001$ vs control) were apparent at the 3-mg/kg dose level. In contrast, rituximab failed to induced significant tumor growth delays in rituximab-resistant Raji-2R (Figure 5B, 0 of 8 CRs, $P = .50$ vs control) but was weakly active in Raji-4RH tumors (Figure 5C; 0 of 8 CRs, $P = .01$ vs control). As expected, rituximab induced more profound tumor growth delays in parental Raji tumors (Figure 5A, 1 of 10 DR, $P < .001$ vs control). Confirming previous observations, we found a strong reduction of the proapoptotic proteins, Bax and Bak, in both rituximab-resistant Raji cells lines (Figure 5C)[24] relative to the parental cell line.[24] In all experiments, rituximab was administered at doses and schedule-inducing maximal pharmacologic effects (data not shown).

In conclusion, our findings demonstrate that hBU12-vcMMAE is highly active in 3 different models of rituximab-resistant NHL tumors. Importantly, the antitumor activity was not significantly affected by alterations in the expression of Bax, Bak, and Bcl-XL, which were previously shown to be associated with resistance of these Raji cell lines against a variety of chemotherapeutic agents.[24]

Discussion

Factors determining the efficacy and potency of hBU12-vcMMAE

The antitumor activities of ADCs are dependent on several biologic parameters, including target biology and the tumor environment, in addition to the physicochemical properties of the drug conjugates.[35] Among the most critical features defining the antitumor effects of ADCs are the cell surface antigen expression levels,[41] internalization kinetics, and intracellular trafficking properties. Rapid internalization and trafficking to the lysosomal compartment in tumor cells[16,42] enable the release of free drug, which is required for the antitumor effects of auristatin-based ADCs.[13,15,43]

Previous studies with different anti-CD19 antibodies revealed differences in their intracellular trafficking to the lysosomes, suggesting that antibody-specific characteristics, such as binding epitopes, binding affinities, internalization kinetics, and their ability to induce CD19 oligomerization, may affect ADC potency.[12,14,41,42] Furthermore, the internalization of a maytansinoid-based anti-CD19 ADC to the lysosomal compartment correlated negatively with CD21 expression levels, and a reduction in antitumor activities against $CD21^{high}$ lymphoma cells grown in culture was reported.[15] In contrast, the potency of PE P38-based anti-CD19 ADCs did not appear to be affected by CD21 expression levels.[14] Based on these observations, we sought to investigate the magnitude of CD21 interference with the potency of the hBU12-vcMMAE conjugate. Our studies revealed rapid internalization and release of free auristatin drugs in several $CD21^{high}$ cell lines exposed to hBU12-vcMMAE, suggesting broad utility for the treatment of NHL, CLL, and ALL tumors irrespective of CD21 expression.

Given the significant differences in the chemical compositions of auristatin, maytansinoid, and PE38-based ADCs, variations in their potencies are probable. In support of this notion, we noticed a 500- and 1000-fold lower potency of the tubulin-blocking maytansinoid DM-1 conjugate and P38-based conjugates, respectively, compared with hBU12-vcMMAE when tested against Ramos cells grown in culture (Table 1).[14,15] Combined, these observations suggest that tumor-intrinsic differences in the sensitivity toward cytotoxic agents may affect ADC potency more prominently than variations in their CD21 expression levels.

Experimental evidence for broader therapeutic utility of hBU12-vcMMAE was provided by the robust antitumor effects observed in 15 of 17 tumor cell lines tested, representing NHL, CLL, and ALL tumors. Tumor inhibition was independent of the CD19 and CD21 expression levels and/or rituximab sensitivities of the tumor cell lines (Table 1). In vitro, neither the amounts of free drug released nor the subcellular localization of ADCs, nor the sensitivity of tumor cell lines toward free MMAE drug, correlated with the potency of hBU12-vcMMAE. Therefore, the differences in drug sensitivity between human tumor cell lines may be caused by other, yet unidentified, mechanisms. Several resistance mechanisms affecting the potencies of tubulin-targeting agents such as taxanes were described, including the up-regulation of aurora kinases, tubulin acetylation, and *tubulin beta III* isoform overexpression.[44,45] However, it remains to be determined whether these mechanisms also account for the differences in sensitivities of different NHL cell lines toward the auristatin-based ADCs identified in this report. It is worth noting that the vcMMAE drug linker is also used in the context of the anti-CD30 antibody cAC10, which induced completed responses in approximately one-third of patients treated in a phase 1 clinical study, validating this class of drug linker to interfere effectively with human B-cell malignancies.[46]

Rituximab resistance mechanisms and the need for novel therapeutics for the treatment of relapsed lymphomas

Rituximab is a chimeric anti-CD20 antibody inducing potent antitumor effects against B-cell lymphomas[47] and is currently used as first-line therapy in combination with chemotherapy for the treatment of most CD20-positive NHLs.[18] However, in patients

with relapsed or refractory disease, rituximab was active in only 50% to 60% of follicular lymphoma and 10% to 15% of small lymphocytic lymphoma patients, even though most tumors were $CD20^+$.[48] Among patients with indolent lymphomas that initially responded to rituximab treatment, only 40% responded to a second cycle of rituximab despite the presence of CD20 on most tumors.[19] Furthermore, some lymphomas do not express CD20 or, alternatively, down-regulate CD20 after rituximab treatment in up to 50% of NHL patients was reported.[21,49,50] In contrast, CD19 expression levels were unaltered in relapsed NHL patients, suggesting that hBU12-vcMMAE may be suitable for the treatment of these patients.

To test the potential impact of rituximab resistance on the activity of hBU12-vcMMAE, we tested 3 resistant NHL cell lines for their response to treatment. The Burkitt lymphoma cell lines, Raji-2R and Raji-4RH, were previously shown to display alterations in the expression of the antiapoptotic protein Bcl-xL and the proapoptotic proteins Bax and Bak.[22,24] Importantly, an association between these molecular changes and cross-resistance toward several chemotherapeutic agents was noticed in these cell lines.[22,24] Unexpectedly, our experiments demonstrate that the antitumor activity of hBU12-vcMMAE is not affected by such cross-resistance. Indeed, similar amounts of free MMAE were released by rituximab-sensitive and -resistant tumors (Table 2), and comparable or improved tumor growth delays were observed in 3 rituximab-resistant NHL models treated with hBU12-vcMMAE relative to rituximab-sensitive tumors.

Despite these encouraging findings, the relevance of our preclinical findings for NHL and ALL patients remains to be determined in clinical trials. In the meantime, our initial data suggest that hBU12-vcMMAE represents a promising new treatment option for first line or advanced patients, who are refractory to standard of care treatment.

Acknowledgments

The authors thank Francisco Zapata, Gerald Neslund, and Bhaskar Rege for conducting and analyzing the pharmacokinetic study with hBU12 compounds and Chuck Cerveny, Django Sussman, and Kristine Kim for their contributions to generate hBU12.

Authorship

Contribution: H.-P.G. designed research, analyzed and interpreted data, and wrote the manuscript; M.K.-S., I.S., C.M.-T., J.M., R.M., S.C.A., N.O., B.H., C.F.M, and P.J.C. designed and performed research, analyzed and interpreted data, and contributed to the writing; D.B. and I.S.G. analyzed and interpreted data; and F.J.H.-I. contributed vital new cell lines and wrote the manuscript.

Conflict-of-interest disclosure: H.-P.G., M.K.-S., I.S., C.M.-T., J.M., R.M., S.C.A., N.O., D.B., and I.S.G. are employees of Seattle Genetics. The remaining authors declare no competing financial interests.

Correspondence: Hans-Peter Gerber, Department of Translational Biology, Seattle Genetics Inc, 21823 30th Dr SE, Bothell, WA 98021; e-mail: hgerber@seagen.com.

References

1. Fearon DT, Carroll MC. Regulation of B lymphocyte responses to foreign and self-antigens by the CD19/CD21 complex. Annu Rev Immunol. 2000;18:393-422.
2. Tedder TF, Zhou LJ, Engel P. The CD19/CD21 signal transduction complex of B lymphocytes. Immunol Today. 1994;15:437-442.
3. Maecker HT, Levy S. Normal lymphocyte development but delayed humoral immune response in CD81-null mice. J Exp Med. 1997;185:1505-1510.
4. Miyazaki T, Muller U, Campbell KS. Normal development but differentially altered proliferative responses of lymphocytes in mice lacking CD81. EMBO J. 1997;16:4217-4225.
5. Engel P, Zhou LJ, Ord DC, Sato S, Koller B, Tedder TF. Abnormal B lymphocyte development, activation, and differentiation in mice that lack or overexpress the CD19 signal transduction molecule. Immunity. 1995;3:39-50.
6. Tedder TF, Clement LT, Cooper MD. Expression of C3d receptors during human B cell differentiation: immunofluorescence analysis with the HB-5 monoclonal antibody. J Immunol. 1984;133:678-683.
7. Yazawa N, Hamaguchi Y, Poe JC, Tedder TF. Immunotherapy using unconjugated CD19 monoclonal antibodies in animal models for B lymphocyte malignancies and autoimmune disease. Proc Natl Acad Sci U S A. 2005;102:15178-15183.
8. Nadler LM, Anderson KC, Marti G, et al. B4, a human B lymphocyte-associated antigen expressed on normal, mitogen-activated, and malignant B lymphocytes. J Immunol. 1983;131:244-250.
9. Uckun FM, Jaszcz W, Ambrus JL, et al. Detailed studies on expression and function of CD19 surface determinant by using B43 monoclonal antibody and the clinical potential of anti-CD19 immunotoxins. Blood. 1988;71:13-29.
10. San Miguel JF, Vidriales MB, Ocio E, et al. Immunophenotypic analysis of Waldenstrom's macroglobulinemia. Semin Oncol. 2003;30:187-195.
11. Ghetie MA, Picker LJ, Richardson JA, Tucker K, Uhr JW, Vitetta ES. Anti-CD19 inhibits the growth of human B-cell tumor lines in vitro and of Daudi cells in SCID mice by inducing cell cycle arrest. Blood. 1994;83:1329-1336.
12. Ghetie MA, Podar EM, Ilgen A, Gordon BE, Uhr JW, Vitetta ES. Homodimerization of tumor-reactive monoclonal antibodies markedly increases their ability to induce growth arrest or apoptosis of tumor cells. Proc Natl Acad Sci U S A. 1997;94:7509-7514.
13. Pulczynski S, Boesen AM, Jensen OM. Antibody-induced modulation and intracellular transport of CD10 and CD19 antigens in human B-cell lines: an immunofluorescence and immunoelectron microscopy study. Blood. 1993;81:1549-1557.
14. Du X, Beers R, Fitzgerald DJ, Pastan I. Differential cellular internalization of anti-CD19 and -CD22 immunotoxins results in different cytotoxic activity. Cancer Res. 2008;68:6300-6305.
15. Ingle GS, Chan P, Elliott JM, et al. High CD21 expression inhibits internalization of anti-CD19 antibodies and cytotoxicity of an anti-CD19-drug conjugate. Br J Haematol. 2008;140:46-58.
16. Press OW, Howell-Clark J, Anderson S, Bernstein I. Retention of B-cell-specific monoclonal antibodies by human lymphoma cells. Blood. 1994;83:1390-1397.
17. Sapra P, Allen TM. Internalizing antibodies are necessary for improved therapeutic efficacy of antibody-targeted liposomal drugs. Cancer Res. 2002;62:7190-7194.
18. Cvetkovic RS, Perry CM. Spotlight on rituximab in non-Hodgkin lymphoma and chronic lymphocytic leukemia. BioDrugs. 2006;20:253-257.
19. Davis TA, Grillo-Lopez AJ, White CA, et al. Rituximab anti-CD20 monoclonal antibody therapy in non-Hodgkin's lymphoma: safety and efficacy of re-treatment. J Clin Oncol. 2000;18:3135-3143.
20. Maloney DG. Immunotherapy for non-Hodgkin's lymphoma: monoclonal antibodies and vaccines. J Clin Oncol. 2005;23:6421-6428.
21. Smith MR. Rituximab (monoclonal anti-CD20 antibody): mechanisms of action and resistance. Oncogene. 2003;22:7359-7368.
22. Czuczman MS, Olejniczak S, Gowda A, et al. Acquirement of rituximab resistance in lymphoma cell lines is associated with both global CD20 gene and protein down-regulation regulated at the pretranscriptional and posttranscriptional levels. Clin Cancer Res. 2008;14:1561-1570.
23. Jazirehi AR, Vega MI, Bonavida B. Development of rituximab-resistant lymphoma clones with altered cell signaling and cross-resistance to chemotherapy. Cancer Res. 2007;67:1270-1281.
24. Olejniczak SH, Hernandez-Ilizaliturri FJ, Clements JL, Czuczman MS. Acquired resistance to rituximab is associated with chemotherapy resistance resulting from decreased Bax and Bak expression. Clin Cancer Res. 2008;14:1550-1560.
25. Alas S, Bonavida B. Rituximab inactivates signal transducer and activation of transcription 3 (STAT3) activity in B-non-Hodgkin's lymphoma through inhibition of the interleukin 10 autocrine/paracrine loop and results in down-regulation of Bcl-2 and sensitization to cytotoxic drugs. Cancer Res. 2001;61:5137-5144.
26. Jazirehi AR, Vega MI, Chatterjee D, Goodglick L, Bonavida B. Inhibition of the Raf-MEK1/2-ERK1/2 signaling pathway, Bcl-xL down-regulation, and chemosensitization of non-Hodgkin's lymphoma B cells by Rituximab. Cancer Res. 2004;64:7117-7126.
27. Bradbury LE, Goldmacher VS, Tedder TF. The

CD19 signal transduction complex of B lymphocytes: deletion of the CD19 cytoplasmic domain alters signal transduction but not complex formation with TAPA-1 and Leu 13. J Immunol. 1993; 151:2915-2927.

28. Matsumoto AK, Martin DR, Carter RH, Klickstein LB, Ahearn JM, Fearon DT. Functional dissection of the CD21/CD19/TAPA-1/Leu-13 complex of B lymphocytes. J Exp Med. 1993;178:1407-1417.
29. Sutherland MS, Sanderson RJ, Gordon KA, et al. Lysosomal trafficking and cysteine protease metabolism confer target-specific cytotoxicity by peptide-linked anti-CD30-auristatin conjugates. J Biol Chem. 2006;281:10540-10547.
30. Flavell DJ, Flavell SU, Boehm DA, et al. Preclinical studies with the anti-CD19-saporin immunotoxin BU12-SAPORIN for the treatment of human-B-cell tumours. Br J Cancer. 1995;72:1373-1379.
31. Sun MM, Beam KS, Cerveny CG, et al. Reduction-alkylation strategies for the modification of specific monoclonal antibody disulfides. Bioconjug Chem. 2005;16:1282-1290.
32. Toki BE, Cerveny CG, Wahl AF, Senter PD. Protease-mediated fragmentation of p-amidobenzyl ethers: a new strategy for the activation of anticancer prodrugs. J Org Chem. 2002;67:1866-1872.
33. Doronina SO, Toki BE, Torgov MY, et al. Development of potent monoclonal antibody auristatin conjugates for cancer therapy. Nat Biotechnol. 2003;21:778-784.
34. Teicher BA, Andrews PA. Anticancer Drug Development Guide (2nd Ed). Totowa, NJ: Humana Press; 2004.
35. Carter PJ. Potent antibody therapeutics by design. Nat Rev Immunol. 2006;6:343-357.
36. Bezombes C, Grazide S, Garret C, et al. Rituximab antiproliferative effect in B-lymphoma cells is associated with acid-sphingomyelinase activation in raft microdomains. Blood. 2004;104:1166-1173.
37. Golay J, Manganini M, Facchinetti V, et al. Rituximab-mediated antibody-dependent cellular cytotoxicity against neoplastic B cells is stimulated strongly by interleukin-2. Haematologica. 2003; 88:1002-1012.
38. Law CL, Cerveny CG, Gordon KA, et al. Efficient elimination of B-lineage lymphomas by anti-CD20-auristatin conjugates. Clin Cancer Res. 2004;10:7842-7851.
39. Hamblett KJ, Senter PD, Chace DF, et al. Effects of drug loading on the antitumor activity of a monoclonal antibody drug conjugate. Clin Cancer Res. 2004;10:7063-7070.
40. Doronina SO, Mendelsohn BA, Bovee TD, et al. Enhanced activity of monomethylauristatin F through monoclonal antibody delivery: effects of linker technology on efficacy and toxicity. Bioconjug Chem. 2006;17:114-124.
41. Carter P, Smith L, Ryan M. Identification and validation of cell surface antigens for antibody targeting in oncology. Endocr Relat Cancer. 2004;11: 659-687.
42. Press OW, Farr AG, Borroz KI, Anderson SK, Martin PJ. Endocytosis and degradation of monoclonal antibodies targeting human B-cell malignancies. Cancer Res. 1989;49:4906-4912.
43. Polson AG, Yu SF, Elkins K, et al. Antibody-drug conjugates targeted to CD79 for the treatment of non-Hodgkin lymphoma. Blood. 2007;110:616-623.
44. Agnese V, Bazan V, Fiorentino FP, et al. The role of Aurora-A inhibitors in cancer therapy. Ann Oncol. 2007;18[suppl 6]:47-52.
45. Parissenti AM, Hembruff SL, Villeneuve DJ, Veitch Z, Guo B, Eng J. Gene expression profiles as biomarkers for the prediction of chemotherapy drug response in human tumour cells. Anticancer Drugs. 2007;18:499-523.
46. Younes A, Forero-Torres A, Bartlett NL, et al. Objective responses in a phase I dose-escalation study of SGN-35, a novel antibody-drug conjugate (ADC) targeting CD30, in patients with relapsed or refractory Hodgkin lymphoma [abstract]. Am Soc Clin Oncol Annual Meeting. 2008; 8526.
47. James JS, Dubs G. FDA approves new kind of lymphoma treatment: Food and Drug Administration. AIDS Treat News. 1997:2-3.
48. McLaughlin P, Grillo-Lopez AJ, Link BK, et al. Rituximab chimeric anti-CD20 monoclonal antibody therapy for relapsed indolent lymphoma: half of patients respond to a four-dose treatment program. J Clin Oncol. 1998;16:2825-2833.
49. Seliem RM, Freeman JK, Steingart RH, Hasserjian RP. Immunophenotypic changes and clinical outcome in B-cell lymphomas treated with rituximab. Appl Immunohistochem Mol Morphol. 2006;14:18-23.
50. Chu PG, Chen YY, Molina A, Arber DA, Weiss LM. Recurrent B-cell neoplasms after Rituximab therapy: an immunophenotypic and genotypic study. Leuk Lymphoma. 2002;43:2335-2341.